The Protein Journal (2023) 42:253–262
https://doi.org/10.1007/s10930-023-10103-x

A Significant Difference in Core PDZ Interactivity of SARS-CoV, SARS-CoV2 and MERS-CoV Protein E Peptide PDZ Motifs In Vitro

Martina Baliova[1] · Iveta Jahodova[1] · Frantisek Jursky[1]

Accepted: 1 March 2023 / Published online: 17 March 2023

Abstract
Small structural E protein of coronaviruses uses its C-terminal PDZ motif to compromise the cellular PDZ interactome. In this work we compared core PDZ interactivity of small (seven amino acids) peptide PDZ motifs, originating from the envelope proteins of recently transmitted coronaviruses SARS-CoV, SARS-CoV2, and MERS-CoV. As the interaction targets we used 23 domains of the largest PDZ proteins MUPP1/MPDZ and PATJ/INAD. Results revealed exceptional affinity and interaction promiscuity of MERS-CoV PDZ motif in vitro, suggesting an increased probability of potential PDZ targets in vivo. We hypothesize that together with its known ability to enter the cells from both apical and basolateral sites, this might further contribute to its elevated disruption of cellular PDZ pathways and higher virulence.

Keywords SARS-CoV · SARS-CoV2 · MERS-CoV · PDZ · MUPP1 · PATJ

1 Introduction

Coronaviruses create a diverse family of enveloped, positive-sense RNA viruses that infect birds and mammals. While the alpha- and betacoronaviruses mainly circulate in bat and rodent reservoirs, the gamma- and deltacoronaviruses have birds as their main reservoir species [1, 2]. Recently, great interest is focused mainly on pathogenic human coronaviruses MERS-CoV, SARS-CoV, and SARS-CoV2, due to their recent zoonotic transmissions [3–5]. The CoVs genome comprises 6–10 open reading frames (ORFs) involved in encoding 16 non-structural proteins (NSP 1–16), four major structural proteins—spike (S), envelope (E), membrane (M), and nucleocapsid (N) protein and five to eight accessory proteins [6].

The envelope glycoprotein (E) is the smallest structural component of SARS-CoVs and plays an essential role in the viral replication, beginning from envelope formation to assembly. It is abundantly expressed in an infected cell, but only a small portion is incorporated into the virion envelope [7, 8]. High expression of protein E, its ability to create homopentameric cationic channels allow viruses to take control over the membrane permeability of endoplasmic reticulum-Golgi complex, which stimulate the virus propagation [9, 10].

Protein E contains a short 3–4 amino-acid long PDZ-binding motif (PBM), allowing its interaction with a conserved module of PDZ (PSD-95/Discs-large/ZO-1) protein domains [11], present in a large number of mainly regulatory proteins [12]. PDZ domain is a structurally highly conserved globule of approximately 90 amino acids folded into six β-sheets (βA–βF) and two α-helices (αA–αB) [13]. PBM is often but not always found at the carboxyl terminus of proteins [14]. Typically major PDZ interaction between motif and domain occurs in the PDZ interaction cavity created by βB sheet, αB helix and carboxylate binding loop [13]. The PDZ domain protein family plays a key role in multicellular organisms, where the PDZ domains are often found as components of multidomain scaffolding proteins involved in cell polarity and intercellular interactions [15, 16]. The PDZ domains are often embedded in proteins present in epithelial junctions [17], neuronal postsynaptic densities [18], and immunological synapses of T cells [19].

The presence of the PDZ binding motif represents the common strategy of viruses that can bind directly to multiple cellular PDZ proteins to increase viral replication

✉ Frantisek Jursky
Frantisek.Jursky@savba.sk

Martina Baliova
Martina.Baliova@savba.sk

[1] Laboratory of Neurobiology, Institute of Molecular Biology, Slovak Academy of Sciences, Dubravska Cesta 21, 845 51 Bratislava, Slovakia

and spread, and represents a determinant of viral pathogenesis [20, 21]. The proteins containing PBMs encoded by different viruses such as influenza A virus, tick-borne encephalitis virus (TBEV) and human papillomavirus (HPV) enhanced virus pathogenesis by interacting with cellular proteins containing PDZ domains, by altering processes such as apoptosis, cell polarity, or innate immune responses [20]. Although the exact role of these interactions in SARS and MERS infections is not well established, there is evidence about SARS-CoV E protein PBM as a virulence factor [21]. In the infection with recombinant viruses lacking an E protein, PBM was attenuated in mice, which was accompanied by a decreased expression of inflammatory cytokines during infection, and a substantial increase of survival [21].

Several PDZ binding partners of SARS-CoV and SARS-CoV2 protein E have been previously identified. One of the protein E interaction partners of SARS-CoV is the cellular protein syntenin 1 [21]. This interaction activates the overexpression of inflammatory cytokines and SARS-CoV lacking E protein PDZ binding motif has decreased expression of inflammatory cytokines, which attenuates virus pathogenicity [21]. Another target of the E protein PDZ binding motif is PALS1, a protein that belongs to the polarity complex Crumbs [22–26]. The E protein relocalizes PALS1 outside the tight junction, altering polarity establishment in epithelial cells. The interaction between PALS1 and protein E could play a key role in the SARS-CoV pathology by altering the integrity of the lung epithelial cells [27, 28]. In addition to the above-mentioned interactions, PDZ tight junction protein ZO1 has been recently identified as a SARS-CoV2 protein E interaction partner [29]. Caillet-Saguy et al. [30] used a high-throughput approach to reveal some additional SARS-CoV2 protein E PDZinteractions.

In this article, we probed MUPP1 also named MPDZ protein [31] and its homologue PATJ/INAD [32, 33] for their potential PDZ interactivity with the SARS-CoV, SARS-CoV2, and MERS-CoV protein E PDZmotifs. Our previous results showed that a core PDZ motif interactivity is relatively promiscuous, suggesting that in vivo might be switched on/off by so far unidentified allosteric structural changes of protein complexes [34]. To identify as many PDZ interactions as possible, regardless of their occurrence in vivo; we used last seven amino acids of the C-terminus of the viral E protein. As a source of library of PDZ domains, we used the largest multi-PDZ proteins PDZ domain proteins, MUPP1 and PATJ, because of the large number of heterologous PDZ domains accumulated in their molecules. We thought that these domains likely represent a wide spectrum of PDZ interactivity, which might help characterize the potency and promiscuity of core viral PDZ motifs which might have relationship with their virulence.

2 Materials and methods

2.1 Preparation of PDZ Domain Fusion Proteins

For the expression of mouse MUPP1, PATJ, and human MUPP1 PDZ domains, mostly EcoRI/SalI (E/S) PCR fragments were inserted into pGEX-5X-1 plasmid (GE Healthcare, Freiburg, Germany) or pGEX-P15A [35] in frame with the glutathione-S-transferase (GST) coding sequence. In the case of the present EcoRI or SalI in internal parts of cloned regions, EcoRI/XhoI (E/X) or BamHI/SalI (B/S) restriction enzyme pairs were used instead. GST fusion proteins containing mouse MUPP1 PDZ domains were used as previously described [36]. For mouse, MUPP1 PDZ domains and regions contained the following amino acid regions: PDZ1(E/S)(G133–P232), PDZ2(E/S)(S231–S347), shorter form, equal to human PDZ2(E/S)(Q254-T342), PDZ3(E/S)(T351–S466), PDZ4(E/S)(K533–I631), PDZ5(E/S)(M667–L782), PDZ6(E/S)(Q990–H1081), PDZ7(E/S)(A1130–R1235), PDZ8(E/S)(L1332–V1429), PDZ9(E/S)(S1464–S1560), PDZ10(E/S)(F1598–P1699), PDZ11(E/S)(E1702–S1812), shorter form equal to human PDZ11(E/S)(C1706-F1796), PDZ12(E/S)(A1839–H1941), PDZ13(E/S)(T1953–S2055), tandem of the first five domain mMUPP1N(PDZ1-5)(E/S)(M1-D794), tandem of last five domains mMUPP1(PDZ9-13)(E/S)((S1464-S2055) (Used numbering is: UniProtKB: Q8VBX6 (MPDZ_MOUSE)).

For the GST fusion proteins containing human MUPP1 PDZ domains, total human cDNA was prepared by RT-PCR amplification from human neuroblastoma cells (SH-SY5Y). PCR DNA fragments corresponding to human MUPP1 protein sequences were obtained by PCR amplification as follows: PDZ1(E/S)(R133-L228), PDZ2(E/S)(Q253-R341), PDZ3(E/S)(S373-E467), PDZ4(E/S)(Y549-T638), PDZ5(E/S)(E695-S790), PDZ6(E/S)(S1004-H1093), PDZ7(E/S)(N1147-R1247), PDZ8(E/S)(G1346-N1437), PDZ9(E/S)(K1479-Q1568), PDZ10(E/S)(G1625-K1716), PDZ11(E/S)(C1721-F1811), PDZ12(E/S)(Q1858-V1952), PDZ13(E/S)(P1983-S2070), tandem of the first five domains hMUPP1N(PDZ1-5)(E/S)(M1-D801), tandem of last five domains hMUPP1(PDZ9-13)(E/S)(K1479- S2070) and tandem of domains 9–11(E/S)(K1479-F1811). (Used numbering is: UniProtKB: O75970 (MPDZ_HUMAN)).

For the GST fusion proteins containing mouse PATJ (INAD) PDZ domains, total mouse cDNA was obtained by RT-PCR amplification from mouse neuroblastoma cells (N2a). PCR DNA fragments corresponding to mouse PATJ PDZ domains protein sequences were obtained by PCR amplification as follows: PDZ1(E/S)(E117-V221), PDZ2(B/S)(P238-T338), PDZ3(E/S) (Y364-K453),

PDZ4(E/X)(E528-L641), PDZ5(E/S)(L679-P774), PDZ6(E/S)(P1072-S1166), PDZ7(E/S)(P1240-M1334), PDZ8(E/S)(E1470-E1555), PDZ9(E/S)(N1563-R1650), PDZ10(E/S)(P1707-N1796). (Used numbering is: UniProtKB: Q63ZW7 (INADL_MOUSE).

2.2 Preparation of Fusion Proteins Containing Viral Protein E PDZ Motifs

Complementary EcoRI-SalI flanked DNA oligonucleotides coding for 7 amino acids viral PDZ motifs SARS-CoV(-GVPDLLV), SARS-CoV2(-RVPDLLV), and MERS-CoV(-LPPDEWV) were synthesized and equimolar amounts of them were annealed by boiling for 5 min and stepwise cooling to room temperature. Complementary strands were designed in such a way that after annealing DNA duplex contained digested EcoRI in the beginning and digested SalI in its end, with preceding TAG protein stop codon. EcoRI/SalI flanked DNA fragments, coding for peptides corresponding to the C-terminus of the SARS CoV2 E protein peptide 1 (-PSFYVYSRVKNLNSSRVPDLLV) and peptide 2(-VSLVKPSFYVYSRVKNLNSSRVPDLLV) were prepared by stepwise PCR extension of short primers. The sequence of SARC CoV2 corresponds to sequence entry: NCBI Reference Sequence: NC_045512.2. It contains a single introduced mutation T198C to eliminate EcoRI in the original sequence, which did not change the protein-coding. DNAs were inserted into EcoRI/SalI digested, frame shifted, pET34b(+) (The original plasmid was +1 frame-shifted by insertion of one cytosine residue between BamHI and EcoRI) or pGEX-P15 [35]. Constructs were transformed into *E. coli* BL21.

2.3 Protein Expression and Purification

E. coli BL21 transformed with plasmid DNA were inoculated into a small volume (20 ml) of LB and shaken (180 rpm) overnight at 37 °C. Culture (3 or 6 ml) was then inoculated into a larger 100 or 250 ml volume of LB. After shaking 2 h at 37 °C (180 rpm) incubation temperature was decreased to 16 °C, and after 30 min, IPTG was added to the final 0.3 mM. Afterward, the culture was shaken overnight. The next day, cells were centrifuged, suspended in lysis buffer A (25 mM Tris–HCl pH7.4, 150 mM NaCl, 5 mM EDTA pH 7.5, 1% Triton X-100), and sonicated. Following centrifugation, the supernatant was either used as an extract for the pull-down interactions or isolation of fusion proteins on glutathione affinity resin (GST-fusion proteins) or microcrystalline cellulose (CBD-fusion proteins) according to [36].

2.4 Pull-Down Assay from Bacterial Extracts

Crude, overnight induced *E. coli* protein extract was obtained as a supernatant after centrifugation (15 min at 13,000×*g* at 4 °C) of induced and sedimented cells disrupted by sonication in buffer A. For the interaction, 0.03 ml of 50% GST resin was incubated with 1 ml of crude extract for 1 h at room temperature (25 °C). The resin was washed with 4 × 1 ml of interaction buffer A and interaction complexes were eluted by the addition of equal amount of 2× SDS sample buffer (100 mM Tris–HCl pH 6.8, 4% SDS, 20% glycerol, 25 mM EDTA, 0.04% Bromphenol Blue, 2% 2-mercapto ethanol). Samples were resolved in 12% PAGE (Acrylamide/BIS 19:1) and visualized by the hot colloidal Coomassie G-250/HCl solution according to [37]. In some cases, the gels were scanned, and the relative intensities of scanned Coomassie-stained protein bands were quantified using UN-SCAN-IT, Silk Scientific Inc. Utah, USA. The interaction was subsequently analysed and plotted as CBD/GST fusion proteins signal ratio with GraphPad Prism 4.00 for Windows, GraphPad Software, and San Diego, CA, USA. Results represent mean ± SD values from at least three independent experiments.

2.5 MUPP1 Pull-Down Assay from Neuroblastoma N2a Cells

DNA fragment of mCherry protein [38] was obtained by PCR using forward BamHI primer (5'-tggggatcctatggtgagcaagggcgaggag-3') and EcoRI reverse primer (5'-gataggagaattccttgtacagctcgtccatgc-3'). Following digestion, DNA fragment was cloned into BglII/EcoRI digested pEDFPN1D [39]. Ligation compatible BamHI/BglII sites are eliminated during the ligation. Subsequently, mouse MUPP1 UniProtKB—Q8VBX6 (MPDZ_MOUSE) DNA (M1-S2055) was cloned in frame with mCherry protein into this plasmid as EcoRI/SalI fragment, using forward EcoRI primer (5'-acgaattcacgccaccatgttggaaaccatagacaaaaatcg-3') and reverse SalI primer (5'-ctggcgtcgacttcaagagagaaccatgagggtgac-3'). N2a cells (mouse neuroblastoma cell lines obtained from the American Type Culture Collection Rockville, Maryland, USA, maintained in high glucose DMEM with glutamine) were transfected with linear PEI [40]. A 10 cm plate of exponentially growing N2a cells were transfected with 15 µg of plasmid DNA, and the next day medium was exchanged. On the following day, cells were washed with physiological saline and scratched into 2 ml of buffer A containing (25 mM Tris–HCl pH 7.5, 150 mM NaCl, 5 mM EDTA pH 7.4, 1% Triton X-100). After 1 h of incubation on ice, the extract was centrifuged for 15 min at 13,000×*g* at 4 °C. The extract was pre-absorbed 15 min with 0.1 ml of glutathione sepharose at room temperature (25 °C). The extract was then divided into two 1 ml aliquots and rotated

on a rotator for 5 h at 25 °C, either with 0.03 ml interaction resin (GST-PSFYVYSRVKNLNSSRVPDLLV) or control GST resin. Following washing with interaction buffer, proteins were eluted with SDS buffer, resolved on gradient 4–12% polyacrylamide gel, and immunoblotted with rabbit anti-MUPP1C antibodies (Thermo Fisher Scientific) and anti-GST antibodies (Sigma-Aldrich).

3 Results

In this work, we investigated the interactions of PDZ motifs of proteins E from SARS-CoV, SARS-CoV2, and MERS-CoV coronaviruses with all 23 PDZ domains of proteins MUPP1 and PATJ. For this purpose, we adapted a previously developed assay system [36], consisting of a set of GST fusion proteins containing PDZ domains and CBD fusion proteins, linked with the C-terminal PDZ peptide motifs of the E protein of the coronaviruses. The size of the PDZ domains polypeptide chains was chosen in such a way that it contained all structural elements necessary for the formation of functional PDZ domain globule [36]. It is generally accepted that only the last three amino acids of PDZ motifs are directly involved in the interaction with the PDZ domain cavity [15]. In the majority of investigated interactions, we used the last seven amino acids of the C-terminus of the protein E. Such a length of peptide motif should already contain some additional structural information influencing PDZ interaction of the core PDZ motif [41, 42], but it is largely free of high order structural restrains (Fig. 1). The affinity of the interacted proteins was large enough to be detected by Coomassie staining, following the resolution of the interaction complexes in protein SDS gel.

Most of the isolated fusion proteins contained a small number of degradation products. They did not interfere with our pull-down assay, because the amount was either low, or the running position was sufficiently different from the interacting CBD-PDZ motif fusion protein on SDS protein gel (Fig. 1 D, H). Human MUPP1 PDZ domain 7 GST fusion protein in addition to its intact form contained a significant amount of second unidentified protein band marked in Fig. 1E-H by an asterisk. Both these proteins were anti-GST positive (not shown), indicating that they represent an intact and truncated version of the same GST-hPDZ7 protein. Despite the running position of the second (upper) band, does slightly coincide with the position of lower interacting MERS-CoV (CBD-LPPDEWV) fusion protein, the specific interaction can be clearly distinguished also in this case (Fig. 1G).

As shown in Fig. 1, in mouse PDZ motifs of SARS-CoV and SARS-CoV2 interacted with stepwise growing intensity with the first three domains and domain 11.

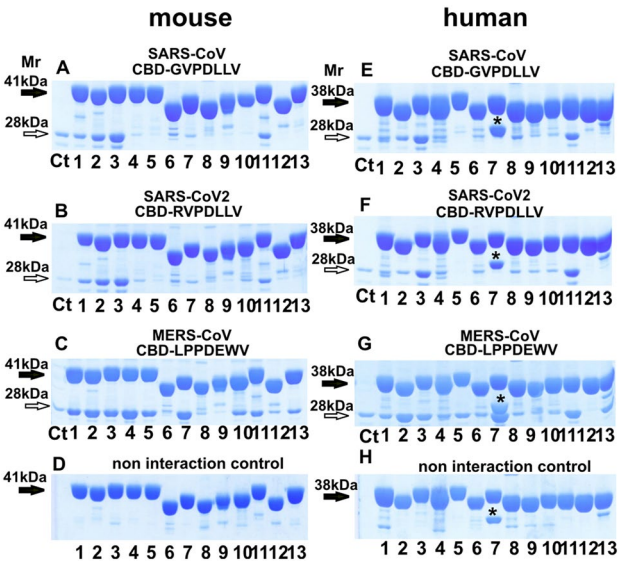

Fig. 1 The PDZ interactions of viral protein E C-terminal peptide motifs with the individual MUPP1 domains. The interaction of mouse and human MUPP1 GST-PDZ domains (1–13) with SARS-CoV (CBD-GVPDLLV) (**A**, **E**), SARS-CoV2 (CBD-RVPDLLV) (**B**, **F**), and MERS-CoV (CBD-LPPDEWV) (**C**, **G**) protein E PDZ motifs fused with CBD protein. Filled arrows indicate GST-PDZ domain (1–13) fusion proteins. The position of the interacting CBD protein band and its running control (Ct) in the first line isolated on microcrystalline cellulose is indicated by open arrows. **D** and **H** show non-interacted control. A significant degradation product in human PDZ domain 7 marked by the asterisk (**E**–**H**)

In human MUPP1, SARS-CoV and SARS-CoV2 PDZ motifs interacted mainly with domains 3 and 11. The interactions with human domain 2 was in comparison with mouse homolog significantly weaker. Even though here used PDZ domains contain all structural elements necessary for folding, a flanking regions of here used human domain 2 are significantly shorter when compared with mouse domain 2 prepared previously [36], (see material and methods). The length of flanking regions is however, unlikely responsible for species interaction differences because they were observed at the level of single, equivalently sized, mouse and human domains 2 (not shown), as well as, equivalently sized, larger mouse and human MUPP1 N-terminal region containing the first five domains (Fig. 2A). The mouse/human amino acid differences are located outside of the PDZ2 interaction cavity. Possible species interaction differences are therefore likely caused by long-distance sterical effects. MERS-CoV interacted individually with all first five domains, domain 7, 10, 11, and domain 13 of mouse and human MUPP1 (Fig. 1C, G). MERS-CoV PDZ motif showed strong association with the N-terminal domain of both mouse and human MUPP1 containing tandem of first five PDZ domains (2A). The interaction was significantly

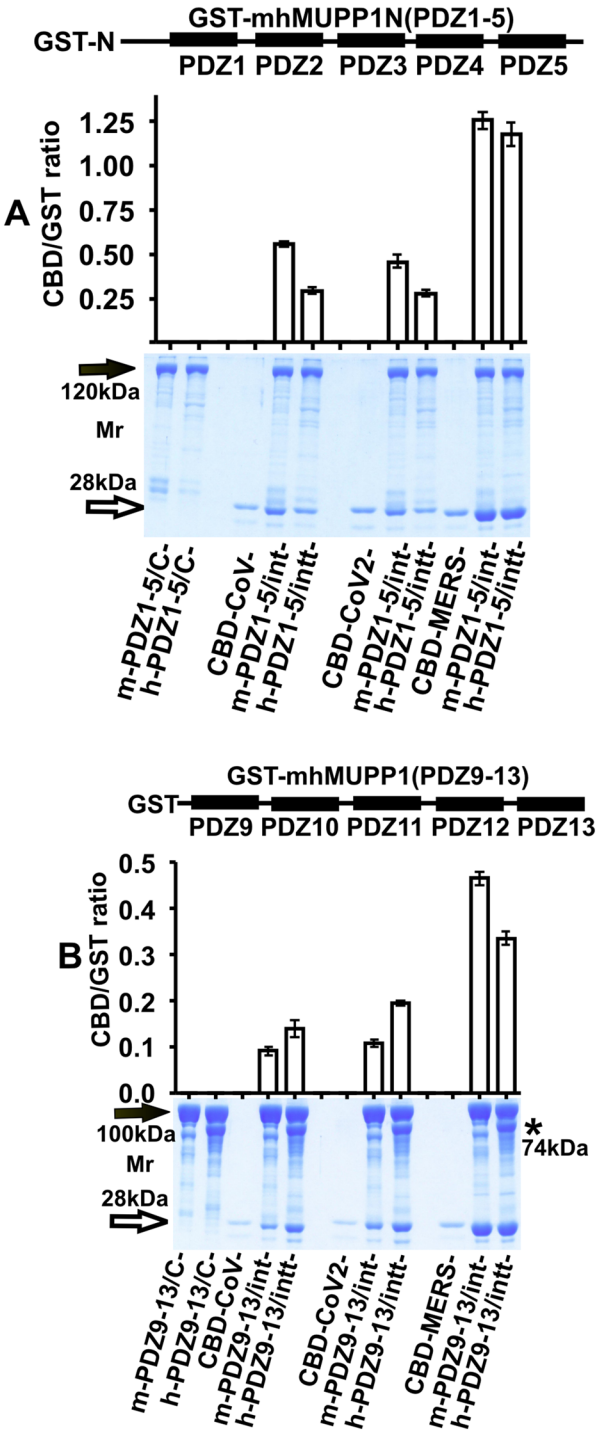

Fig. 2 The PDZ interactions of viral protein E C-terminal peptide motifs with the tandems of MUPP1 domains. The interaction of CBD proteins fused with SARS-CoV, SARS-CoV2, and MERS-CoV PDZ motifs with the GST fusion proteins containing mouse (m) and human (h) equivalently sized MUPP1 N-terminal fragments bearing first five domains [GST-mhMUPP1N(PDZ1-5)] (**A**) and MUPP1 C-terminal fragment bearing last five (9–13) PDZ domains [GST-mhMUPP1(PDZ9-13)] (**B**). The asterisk in B show the position of a degradation product of GST-mhMUPP1(PDZ9-13). The labels C- and int-indicate control and interacted sample, respectively. Filled arrows indicate GST fusion proteins. The position of the interacting CBD protein band and its running control isolated on microcrystalline cellulose is indicated by the opened arrows. The GST and CBD fusion protein interaction partners were quantified by scanning of the stained protein bands and plotted as CBD/GST ratio (see materials and methods for details). Results represent mean ± SD values from three independent experiments

stronger when compared with SARS-CoV and SARS-CoV2 (2A).

In the region of domains 9–13, both mouse and human MUPP1 interacted with SARS-CoV and SARS-CoV2 PDZ motif mainly through domain 11, but MERS-CoV interacted in addition with the mouse domains 10 and 13 and human domain 13 (Fig. 1C, G). The tandem of human C-terminal domains 9–13 revealed much stronger interaction with SARS-CoV and SARS-CoV2 PDZ motifs when compared with mouse homologue (Fig. 2B). On the contrary, MERS-CoV showed slightly weaker interaction with the human MUPP1 (9–13) region when compared with mouse homologue (Fig. 2B). GST fusion protein containing tandem of human PDZ domains 9–13 has a significant amount of degradation product (in Fig. 2B marked by the asterisk). Mobility of degradation product of GST-hMUPP1(9–13) in SDS protein gel is slower than GST-hMUPP1(9–11), indicating that degradation product still contains PDZ domain 11 (not shown). We therefore adjusted the amount of interacting protein to the summarized amount of intact and degraded protein. Results, however, still suggested the higher affinity of SARS-CoV and SARS-CoV2 PDZ motifs to human MUPP1 domains 9–13 in comparison with mouse domains 9–13 (Fig. 2B). Enhanced degradation of human MUPP1 C-terminus containing tandem of PDZ domains 9–13 indicates the presence of sequence/structural determinant making this protein accessible to unknown proteolytic system of *E. coli*. This sequence/structural determinant seems to be not present in mouse MUPP1 C-terminus, and it might result in human MUPP1 specific sterical constraints, explaining the species difference in the interaction between SARS-CoV and SARS-CoV2 PDZ motifs possibly existing in vivo.

In subsequent work, we decided to investigate the interactions of PDZ peptide motifs of coronaviruses with MUPP1 homologue PATJ/INAD [32], which is similar to MUPP1 associated with epithelial tight junctions through its non PDZ interaction with PALS1 [33]. Similar to MUPP1, PATJ interacted with SARS-CoV and SARS-CoV2 PDZ motif mainly through PDZ domains 2 and 3, and domain 9, which is the homologue of MUPP1 domain 11 (Fig. 3). MERS-CoV PDZ motif interacted with PATJ domains 1, 2, 3, 5, 6, and 9. Except for PATJ PDZ domain 4, which differs significantly from the MUPP1 equivalent, the interactions were also very similar, since PATJ domains 6 and 9 are homologues of MUPP1 domains

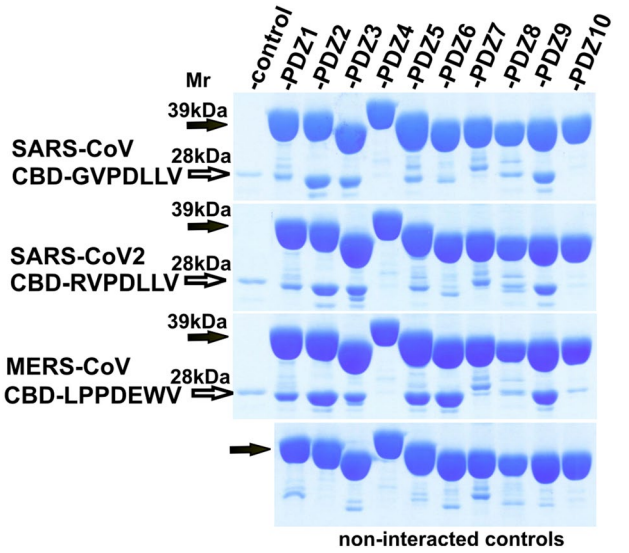

Fig. 3 The PDZ interactions of viral protein E C-terminal peptide motifs with the individual of PATJ/INAD domains. The interaction of mouse PATJ GST-PDZ domains with SARS-CoV (CBD-GVPDLLV), SARS-CoV2 (CBD-RVPDLLV), and MERS-CoV (CBD-LPPDEWV) protein E PDZ motifs fused with CBD protein. Filled arrows indicate GST fusion proteins. The position of the interacting CBD protein band and its running control isolated on microcrystalline cellulose is indicated by the opened arrows. The low panel shows non-interacted controls

7 and 11, respectively (Fig. 3). Summary of the obtained PDZ interactions (Figs. 1, 3) is show on Table 1.

GST and CBD fusion proteins used in this work might introduce unpredictable sterical constraints, which either increase or block the accessibility of PDZ motifs and domains. To investigate if the extension of the 7 amino acids PDZ motif to a longer peptide region and switching the fusion partner will affect the PDZ interaction with MUPP1, we extended the sequences to 22 and 27 amino acids of SARS-CoV2 protein E C-terminus. While the CBD fusion proteins with these peptides were very poorly expressed, their fusion with GST protein as well as a fusion of CBD protein with MUPP1 PDZ domain 3 was expressed well. Results revealed that in this approach out of 7, 22, and 27 amino acids extensions, GST fusion with 22 amino acids extension exhibited the best accessibility of the protein E PDZ motif for the interaction with MUPP1 PDZ domain 3 fused to CBD protein (Fig. 4A). This GST fusion was also able to pull-down intact MUPP1 protein from the protein extract of N2a cells transfected with MUPP1 (Fig. 4B).

Table 1 Summary of the obtained PDZ interactions

mMUPP1	SARS-CoV	SARS-CoV2	MERS-CoV	hMUPP1	SARS-CoV	SARS-CoV2	MERS-CoV	mPATJ/INAD	SARS-CoV	SARS-CoV2	MERS-CoV
PDZ1	+	+	+	PDZ1	+	+	+	PDZ1	+	+	+
PDZ2	+	+	+	PDZ2	+	+	+	PDZ2	+	+	+
PDZ3	+	+	+	PDZ3	+	+	+	PDZ3	+	+	+
PDZ4	–	–	+	PDZ4	–	–	+	PDZ4	–	–	–
PDZ5	–	–	+	PDZ5	–	–	+	PDZ5	–	–	+
PDZ6	–	–	–	PDZ6	–	–	+	PDZ6	–	–	+
PDZ7	–	–	+	PDZ7	–	–	+	PDZ7	–	–	–
PDZ8	–	–	–	PDZ8	–	–	–	PDZ8	–	–	–
PDZ9	–	–	–	PDZ9	–	–	–	PDZ9	+	+	+
PDZ10	–	–	+	PDZ10	–	–	–	PDZ10	–	–	–
PDZ11	+	+	+	PDZ11	+	+	+				
PDZ12	–	–	–	PDZ12	–	–	–				
PDZ13	–	–	+	PDZ13	–	–	+				

Columns show the interactions of GST fusion proteins containing mouse and human MUPP1/MPDZ PDZ domains 1–13 and mPATJ/INAD domains 1–10 with seven amino acids PDZ motifs of SARS-CoV, SARS-CoV2, and MERS-CoV fused with CBD protein. Plus/minus symbols indicate the presence or absence of the interaction, respectively. See figure gels for details

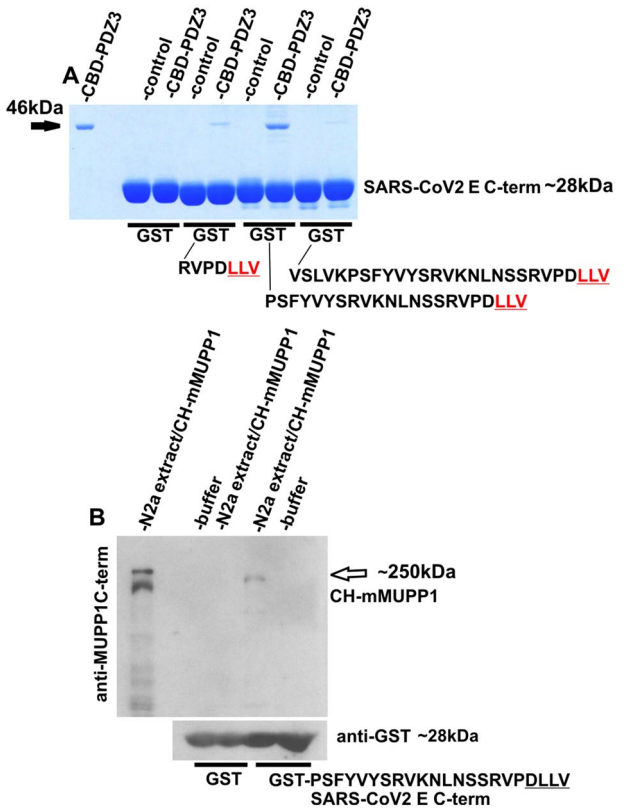

Fig. 4 The PDZ interactions of extended SARS-CoV2 protein E C-terminal peptides motifs. The interaction of mouse MUPP1 PDZ domain 3 (marked by filled arrow) fused to CBD (CBD-PDZ3) with last 7 (-RVPDLLV), 22 (-PSFYVYSRVKNLNSSRVPDLLV), and 27 (-VSLVKPSFYVYSRVKNLNSSRVPDLLV) amino-acids of SARS-CoV2 protein E C-terminus fused with GST protein (**A**). The interaction of mCherry tagged whole mouse MUPP1 (CH-mMUPP1 marked by empty arrow) expressed in N2a cells with the last 22 amino acids (-PSFYVYSRVKNLNSSRVPDLLV) of SARS-CoV2 protein E C-terminus fused with GST protein (**B**). The PDZ binding motif is underlined

4 Discussion

In this work, we show that minimal PDZ motifs represented by last 7 amino acids of protein E C-terminus from SARS-CoV, SARS-CoV2, and MERS-CoV coronaviruses bind to several PDZ domains of proteins MUPP1/MPDZ and PATJ/INAD in vitro (Figs. 1,3, Table 1). The specific interaction of short viral PDZ motifs coupled to bacterial CBD with PDZ domains GST fusion proteins indicates that both motifs and domains were in our experimental conditions freely accessible, folded as functional structural elements allowing specific PDZ interaction to take place. Even though some of the interactions reported here might be prevented by high order macromolecular assemblies of proteins in vivo, their interaction capability might be on the contrary also significantly increased in favor of the PDZ interaction in various cellular and protein conditions. This might include allosteric changes of the accessibility by additional interacting partners or proteolysis leading to the presence of protein E C-terminal peptide fragments in vivo.

In this content, it is worth mentioning that SARS-CoV protein E is produced in the infected cell in large excess, and only a small portion is incorporated into virion [7]. A quick turnover has been reported for SARS-CoV protein E [43], suggesting the possible existence of short peptide PDZ motifs. Some in silico algorithms predict the presence of calpain cleavage sites, and all here investigated viral E proteins contain cleavage sites for trypsin. Trypsin cuts peptide chains mainly at the carboxyl side of the amino acids lysine or arginine not followed by proline [44]. The search of SARS-CoV2 protein sequence indicates potential trypsin cleavage sites in positions 38, 61, 63 and 69. The sites 61, 63, and 69 are located in the distal protein E C-terminus, releasing the peptides 6, 12 and 14 amino acid long, following potential trypsin cleavage. Their size is close to the here used PDZ peptide motifs. Expression of trypsin by epithelial cells of various tissues, leukocytes, and neurons in human and mouse has been previously reported [45]. SARS-CoV2 infects intestinal epithelial cells [46], and gastrointestinal involvement, likely including virus replication, has already been reported for other coronaviruses, including SARS-CoV [47] and the Middle East Respiratory Syndrome (MERS) [48, 49].

Numerous PDZ domains present in multiple PDZ proteins MUPP1/MPDZ and PATJ/INAD interact with several regulatory molecules, including tight junction components, kinases, neurotransmitter receptors and others [50]. Currently, it is therefore difficult to predict the effects of these interactions on cellular systems. For example, spread of coronaviruses, proteins or their fragments by exosomes and extracellular vesicles has been previously proposed by some authors [51, 52]. Additionally, human neuronal cells, normally nonpermissive to endocytic infection, were infected by coculturing them with SARS-CoV2 permissive infected epithelial cells. This happened by the SARS-CoV-2 induced formation of tunneling nanotubes (TNTs) [53].

Shepley-McTaggart et al. [29] previously reported the interaction of SARS CoV2 protein E, biotinylated C-terminal peptide (Biotin-SRVKNLNSSRVPDLLV-COOH) with the PDZ tight junction protein ZO1. The array used in the interaction also contained GST fusion proteins of MUPP1 with domains 5, 10, 11, 12, and 13, but none of these domains interacted in their assay with the SARS-CoV2 PDZ motif. With exception of MUPP1 PDZ domain 11, none of these domains interacted in our assay as well (Fig. 1, Table 1). The authors did not specify the chemistry used for coupling the fusion proteins to the array and the length of the PDZ domains polypeptides used. We think that possible differences in these parameters might modify the accessibility of ligand and explain the discrepancy in the

interaction of domain 11. Recently Caillet-Saguy et al. [30] identified specific interaction of PDZ domain 2, present in LNX2 (Ligand of Numb Protein-X) protein with biotinylated 12 amino acids C-terminal peptide containing PDZ motif of SARS-CoV2 protein E. Four domains of LNX2 are known to be homologues of the last four domains (10–13) of MUPP1 [54]. LNX2 domain 2 is a homologue of MUPP1 domain 11 and PATJ domain 9. LNX2 domain 2 [30], MUPP1 domain 11, and PATJ domain 9 (this work) all interact with SARS-CoV2 (Fig. 1,3, Table 1), which suggests that these interactions might be meaningful.

5 Conclusion

The purpose of this study was to investigate the promiscuity and affinity of minimal PDZ binding motifs of protein E originating from SARS-CoV, SARS-CoV2, and MERS-CoV. The used library of 23 PDZ domains was derived from the largest multi-PDZ proteins MUPP1 and PATJ. Results revealed significantly higher affinity and promiscuity of the MERS-CoV core PDZ motif in comparison to SARS variants. Even though due to size limitation of PDZ motifs not all here identified interactions might occur in vivo, we believe that these differences reflect an increased probability of potential PDZ targets in vivo. We hypothesize that together with the ability of MERS-CoV to enter the cells from both apical and basolateral sites [55], this might contribute to its elevated disruption of cellular PDZ pathways and higher virulence. Here used assay can be potentially used to explore the affinity and promiscuity of other viral PDZ motifs and correlate them with their virulence.

Acknowledgements This work was supported by the VEGA Grant 2/0127/21

Author Contribution MB and FJ contributed towards the conception and design of the study. MB, IJ were responsible for the acquisition of data. MB and IJ performed the pull-down analysis. MB and FJ analysed and interpreted the data, with significant inputs from IJ. All authors have given approval to the final version of the manuscript.

Data Availability Materials, data, and associated protocols are available upon reasonable request.

Declarations

Conflict of interest The authors declare they have no conflict of interest.

References

1. Wille M, Holmes EC (2020) Wild birds as reservoirs for diverse and abundant gamma- and deltacoronaviruses. FEMS Microbiol Rev 44:631–644
2. Artika IM, Dewantari AK, Wiyatno A (2020) Molecular biology of coronaviruses: current knowledge. Heliyon 6:e04743. https://doi.org/10.1016/j.heliyon.2020.e04743
3. Zhong NS, Zheng BJ, Li YM et al (2003) Epidemiology and cause of severe acute respiratory syndrome (SARS) in Guangdong, People's Republic of China, in February, 2003. Lancet 362:1353–1358
4. de Groot RJ, Baker SC, Baric RS, Brown CS, Drosten Ch, Enjuanes L, Fouchier RAM, Galiano M, Gorbalenya AE, Memish ZA, Perlman S, Poon LLM, Snijder EJ, Stephens GM, Woo PCY, Zaki AM, Zambon M, Ziebuhr J (2013) Middle East respiratory syndrome coronavirus (MERS-CoV): announcement of the Coronavirus Study Group. J Virol 87:7790–7792
5. Holmes EC, Goldstein SA, Rasmussen AL, Robertson DL, Crits-Christoph A, Wertheim JO, Anthony SJ, Barclay WS, Boni MF, Doherty PC, Farrar J, Geoghegan JL, Jiang X, Leibowitz JL, Neil SJD, Skern T, Weiss SR, Worobey WuA, Peng Y, Huang B, Ding X, Wang X, Niu P, Meng J, Zhu Z, Zhang Z, Wang J, Sheng J (2020) Genome composition and divergence of the novel coronavirus (2019-nCoV) originating in China. Cell Host Microbe 27:325–328
6. Wu A, Peng Y, Huang B, Ding X, Wang X, Niu P, Meng J, Zhu Z, Zhang Z, Wang J, Sheng J (2020) Genome composition and divergence of the novel coronavirus (2019-nCoV) originating in China. Cell Host Microbe 27:325–328
7. Venkatagopalan P, Daskalova SM, Lopez LA, Dolezal KA, Hogue BG (2015) Coronavirus envelope (E) protein remains at the site of assembly. Virology 478:75–85
8. Schoeman D, Fielding BC (2019) Coronavirus envelope protein: current knowledge. Virol J 16:69. https://doi.org/10.1186/s12985-019-1182-0
9. Wilson L, McKinlay C, Gage P, Ewart G (2004) SARS coronavirus E protein forms cationselective ion channels. Virology 330:322–331
10. Liu DX (2006) Model of a putative pore: the pentameric alpha-helical bundle of SARS coronavirus E protein in lipid bilayers. Biophys J 91:938–947
11. Kennedy MB (1995) Origin of PDZ (DHR, GLGF) domains. Trends Biochem Sci 20:350
12. Chang BH, Gujral TS, Karp ES, BuKhalid R, Grantcharova VP, MacBeath GA (2011) systematic family-wide investigation reveals that ~30% of mammalian PDZ domains engage in PDZ-PDZ interactions. Chem Biol 18:1143–1152. https://doi.org/10.1016/j.chembiol.2011.06.013
13. Doyle DA, Lee A, Lewis J, Kim E, Sheng M, MacKinnon R (1996) Crystal structures of a complexed and peptide-free membrane protein-binding domain: molecular basis of peptide recognition by PDZ. Cell 85:1067–1076
14. Hillier BJ, Christopherson KS, Prehoda KE, Bredt DS, Lim WA (1999) Unexpected modes of PDZ domain scaffolding revealed by structure of nNOS-syntrophin complex. Science 284:812–815
15. Harris BZ, Lim WA (2001) Mechanism and role of PDZ domains in signaling complex assembly. J Cell Sci 114:3219–3231
16. Sheng M, Sala C (2001) PDZ domains and the organization of supramolecular complexes. Annu Rev Neurosci 24:1–29
17. Humbert P, Russell S, Richardson H (2003) Dlg, Scribble and Lgl in cell polarity, cell proliferation and cancer. BioEssays 25:542–553
18. Kim E, Sheng M (2004) PDZ domain proteins of synapses. Nat Rev Neurosci 5:771–781
19. Ludford-Menting MJ, Oliaro J, Sacirbegovic F, Cheah ET, Pedersen N et al (2005) A network of PDZ-containing proteins regulates T cell polarity and morphology during migration and immunological synapse formation. Immunity 22:737–748
20. Javier RT, Rice AP (2011) Emerging theme: cellular PDZ proteins as common targets of pathogenic viruses. J Virol 85:11544–11556

21. Jimenez-Guardeño JM, Nieto-Torres JL, DeDiego ML, Regla-Nava JA, Fernandez-Delgado R, Castaño-Rodriguez C, Enjuanes L (2014) The PDZ-binding motif of severe acute respiratory syndrome coronavirus envelope protein is a determinant of viral pathogenesis. PLoS Pathog 10:e1004320
22. Kamberov E, Makarova O, Roh M, Liu A, Karnak D, Straight S, Margolis B (2000) Molecular cloning and characterization of Pals, proteins associated with mLin-7. J Biol Chem 275:11425–11431
23. Makarova O, Roh MH, Liu CJ, Laurinec S, Margolis B (2003) Mammalian Crumbs3 is a small transmembrane protein linked to protein associated with Lin-7 (Pals1). Gene 302:21–29
24. Chai J, Cai Y, Pang C, Wang L, McSweeney S, Shanklin J, Liu Q (2021) Structural basis for SARS-CoV-2 envelope protein recognition of human cell junction protein PALS1. Nat Commun 12:3433. https://doi.org/10.1038/s41467-021-23533-x
25. Javorsky A, Humbert PO, Kvansakul M (2021) Structural basis of coronavirus E protein interactions with human PALS1 PDZ domain. Commun Biol 4:724. https://doi.org/10.1038/s42003-021-02250-7
26. Lo Cascio E, Toto A, Babini G, De Maio F, Sanguinetti M, Mordente A, Della Longa S, Arcovito A (2021) Structural determinants driving the binding process between PDZ domain of wild type human PALS1 protein and SLiM sequences of SARS-CoV E proteins. Comput Struct Biotechnol J 19:1838–1847. https://doi.org/10.1016/j.csbj.2021.03.014
27. Teoh KT, Siu YL, Chan WL, Schlüter MA, Liu CJ, Peiris JS, Bruzzone R, Margolis B, Nal B (2010) The SARS coronavirus E protein interacts with PALS1 and alters tight junction formation and epithelial morphogenesis. Mol Bio Cell 21:3838–3852. https://doi.org/10.1091/mbc.E10-04-0338
28. DeDiego ML, Nieto-Torres JL, Jimenez-Guardeño JM, Regla-Nava JA, Castaño-Rodriguez C, Fernandez-Delgado R, Usera F, Enjuanes L (2014) Coronavirus virulence genes with main focus on SARS-CoV envelope gene. Virus Res 194:124–137
29. Shepley-McTaggart A, Sagum CA, Oliva I, Rybakovsky E, DiGuilio K, Liang J, Bedford MT, Cassel J, Sudol M, Mullin JM, Harty RN (2021) protein SARS-CoV-2 Envelope (E) protein interacts with PDZ-domain-2 of host tight junction ZO1. PLoS ONE 16:e0251955. https://doi.org/10.1371/journal.pone.0251955
30. Caillet-Saguy C, Durbesson F, Rezelj VV, Gogl G, Tran QD, Twizere JC, Vignuzzi M, Vincentelli R, Wolff N (2021) Host PDZ-containing proteins targeted by SARS-CoV-2. FEBS J 288:5148–5162. https://doi.org/10.1111/febs.15881
31. Ullmer C, Schmuck K, Figge A, Lübbert H (1998) Cloning and characterization of MUPP1, a novel PDZ domain protein. FEBS Lett 424:63–68. https://doi.org/10.1016/s0014-5793(98)00141-0
32. Adachi M, Hamazaki Y, Kobayashi Y, Itoh M, Tsukita S, Furuse M, Tsukita S (2009) Similar and distinct properties of MUPP1 and Patj, two homologous PDZ domain-containing tight-junction proteins. Mol Cell Biol 29:2372–2389. https://doi.org/10.1128/MCB.01505-08
33. Baliova M, Jursky F (2020) Comparison of SynCAM1/CADM1 PDZ interactions with MUPP1 using mammalian and bacterial pull-down systems. Brain Behav 10:e01587. https://doi.org/10.1002/brb3.1587
34. Assémat E, Crost E, Ponserre M, Wijnholds J, Le Bivic A, Massey-Harroche D (2013) The multi-PDZ domain protein-1 (MUPP-1) expression regulates cellular levels of the PALS-1/PATJ polarity complex. Exp Cell Res 319:2514–2525. https://doi.org/10.1016/j.yexcr.2013.07.011
35. Baliova M, Jursky F (2020) Phosphorylation of serine 157 protects the rat glycine transporter GlyT2 from Calpain cleavage. J Mol Neurosci 70:1216–1224. https://doi.org/10.1007/s12031-020-01529-4
36. Baliova M, Juhasova A, Jursky F (2014) Using a collection of MUPP1 domains to investigate the similarities of neurotter transporters C-terminal PDZ motifs. Biochem Biophys Res Commun 454:25–29. https://doi.org/10.1016/j.bbrc.2014.10.011
37. Lawrence AM, Besir HU (2009) Staining of proteins in gels with Coomassie G-250 without organic solvent and acetic acid. J Vis Exp 30:e1350
38. Shaner NC, Campbell RE, Steinbach PA, Giepmans BN, Palmer AE, Tsien RY (2004) Improved monomeric red, orange and yellow fluorescent proteins derived from Discosoma sp. red fluorescent protein. Nat Biotechnol 22:1567–1572
39. Baliova M, Jursky F (2005) Calpain sensitive regions in the N-terminal cytoplasmic domains of glycine transporters GlyT1A and GlyT1B. Neurochem Res 30:1093–1100. https://doi.org/10.1007/s11064-005-7520-1
40. Jeong JH, Song SH, Lim DW, Lee H, Park TG (2001) DNA transfection using linear poly(ethylenimine) prepared by controlled acid hydrolysis of poly(2-ethyl-2-oxazoline). J Control Release 73:391–399
41. Songyang Z, Fanning AS, Fu C, Xu J, Marfatia SM, Chishti AH, Crompton A, Chan AC, Anderson JM, Cantley LC (1997) Recognition of unique carboxyl-terminal motifs by distinct PDZ domains. Science 275:73–77
42. Tonikian R, Zhang Y, Sazinsky SL, Currell B, Yeh JH, Reva B, Held HA, Appleton BA, Evangelista M, Wu Y, Xin X, Chan AC, Seshagiri S, Lasky LA, Sander C, Boone C, Bader GD, Sidhu SS (2008) A specificity map for the PDZ domain family. PLoS Biol 6:e239. https://doi.org/10.1371/journal.pbio.0060239
43. Nal B, Chan CH, Kien F, Siu L, Tse J, Chu K, Kam J, Staropoli I, Crescenzo-Chaigne B, Escriou N, Van der Werf S, Yuen K-Y, Altmeyer R (2005) Differential maturation and subcellular localization of severe acute respiratory syndrome coronavirus surface proteins S, M and E. J Gen Virol 86:1423–1434. https://doi.org/10.1099/vir.0.80671-0
44. Rodriguez J, Gupta N, Smith RD, Pevzner PA (2008) Does trypsin cut before proline? J Proteome Res 1:300–305. https://doi.org/10.1021/pr0705035
45. Koshikawa N, Hasegawa S, Nagashima Y, Mitsuhashi K, Tsubota Y, Miyata S, Miyagi Y, Yasumitsu H, Miyazaki K (1998) Expression of trypsin by epithelial cells of various tissues, leukocytes, and neurons in human and mouse. Am J Pathol 153:937–944. https://doi.org/10.1016/S0002-9440(10)65635-0
46. Lehmann M, Allers K, Heldt C, Meinhardt J, Schmidt F, Rodriguez-Sillke Y, Kunkel D, Schumann M, Böttcher C, Stahl-Hennig C, Elezkurtaj S, Bojarski C, Radbruch H, Corman VM, Schneider T, Loddenkemper C, Moos V, Weidinger C, Kühl AA, Siegmund B (2021) Human small intestinal infection by SARS-CoV-2 is characterized by a mucosal infiltration with activated CD8(+) T cells. Mucosal Immunol 14:1381–1392. https://doi.org/10.1038/s41385-021-00437-z
47. Booth CM, Matukas LM, Tomlinson GA, Rachlis AR, Rose DB, Dwosh HA, Walmsley SL, Mazzulli T, Avendano M, Derkach P, Ephtimios IE, Kitai I, Mederski BD, Shadowitz SB, Gold WL, Hawryluck LA, Rea E, Chenkin JS, Cescon DW, Poutanen SM, Detsky AS (2003) Clinical features and short-term outcomes of 144 patients with SARS in the greater Toronto Area. JAMA 289:2801–2809
48. Assiri A, Al-Tawfiq JA, Al-Rabeeah AA, Al-Rabiah FA, Al-Hajjar S, Al-Barrak A, Flemban H, Al-Nassir WN, Balkhy HH, Al-Hakeem RF, Makhdoom HQ, Zumla AI, Memish ZA (2013) Epidemiological, demographic, and clinical characteristics of 47 cases of Middle East respiratory syndrome coronavirus disease from Saudi Arabia: a descriptive study. Lancet Infect Dis 13:752–761. https://doi.org/10.1016/S1473-3099(13)70204-4
49. Zhou J, Li C, Zhao G, Chu H, Wang D, Yan HH, Poon VK, Wen L, Wong BH, Zhao X, Chiu MC, Yang D, Wang Y, Au-Yeung RKH, Chan IH, Sun S, Chan JF, To KK, Memish ZA, Corman VM, Drosten C, Hung IF, Zhou Y, Leung SY, Yuen KY (2017)

Human intestinal tract serves as an alternative infection route for Middle East respiratory syndrome coronavirus. Sci Adv 3:e4966. https://doi.org/10.1126/sciadv.aao4966
50. Gromova OA, Torshin IY, Semenov VA, Putilina MV, Chuchalin AG (2021) Direct and Indirect Neurological Signs of COVID-19. Neurosci Behav Physiol 4:1–11. https://doi.org/10.1007/s11055-021-01144-9
51. Estrada E (2020) Protein-driven mechanism of multiorgan damage in COVID-19. Med Drug Discov 20:100069. https://doi.org/10.1016/j.medidd.2020.100069
52. Hassanpour M, Rezaie J, Nouri M, Panahi Y (2020) The role of extracellular vesicles in COVID-19 virus infection. Infect Genet Evol 85:104422. https://doi.org/10.1016/j.meegid.2020.104422
53. Pepe A, Pietropaoli S, Vos M, Barba-Spaeth G, Zurzolo C (2022) Tunneling nanotubes provide a route for SARS-CoV-2 spreading. Sci Adv 8:eabo0171. https://doi.org/10.1126/sciadv.abo0171
54. Flynn M, Saha O, Young P (2011) Molecular evolution of the LNX gene family. BMC Evol Biol 11:235. https://doi.org/10.1186/1471-2148-11-235
55. Tao X, Hill TE, Morimoto C, Peters CJ, Ksiazek TG, Tseng CT (2013) Bilateral entry and release of Middle Eastrespiratory syndrome coronavirus induces profound apoptosis of human bronchial epithelial cells. J Virol 87:9953–9958. https://doi.org/10.1128/JVI.01562-13